


 Cite this: *RSC Adv.*, 2022, 12, 26176

# The application of photoelectrocatalysis in the degradation of rhodamine B in aqueous solutions: a review

 Tunde Lewis Yusuf,<sup>a</sup> Benjamin O. Orimolade,<sup>b</sup> Daniel Masekela,<sup>a</sup> Bhekile Mamba<sup>b</sup> and Nonhlangabezo Mabuba<sup>\*a</sup>

The pollution of the water environment by industrial effluents is an ongoing challenge due to the rate of industrialisation and globalisation. Photoelectrocatalysis (PEC), an electrochemical advanced oxidation process, has proven to be an effective method for removing organics from wastewater. Photoelectrocatalysis is environmentally benign, cost-effective and easy to operate. In this present review, we examine the recent progress in the removal of rhodamine B dye, a common constituent of textile effluent released into the environment, through photoelectrocatalytic degradation. We present a detailed discussion on the use of different kinds of unmodified and modified photoanodes that have been explored for the photoelectrocatalytic removal of this dye. More importantly, discussions are presented on the mechanisms and kinetics of the degradation of rhodamine B dye using these photoanodes. Hence, this review will be beneficial for researchers in developing future projects in the area of wastewater treatments through photoelectrocatalysis.

 Received 8th July 2022  
 Accepted 7th September 2022

DOI: 10.1039/d2ra04236c

[rsc.li/rsc-advances](http://rsc.li/rsc-advances)

## 1 Introduction

There are many challenges presently limiting the quality of life and the environment. Among these challenges, the issue of water pollution has remained a significant concern as it is mainly responsible for water scarcity and water stress in both developed and developing societies. The problem of water pollution in recent years can be directly linked to an exponential increase in the rate of urbanization and industrialization.<sup>1</sup> Water pollution can be from natural sources, which could result from natural phenomena such as acid rain or natural disasters like volcanic eruptions. Still, the bulk of water pollution originates from anthropogenic sources such as improper disposal of industrial effluents and household wastes which ultimately end up in surface water and groundwater.<sup>2</sup> It has been noted that water pollutants are diverse, and they include a wide range of heavy metals such as iron, lead, arsenic and selenium.<sup>3</sup> However, many pollutants detected in water are organic in nature and belong to numerous classes. Examples of such organic pollutants include pesticides originating from agricultural activities, pharmaceuticals and personal care products emanating from pharmaceutical industries, hospitals and households, and organic dyes originating from textile industries.<sup>4</sup>

The textile sector remains a robust sector responsible for more than 800 tons of synthetic dyes yearly.<sup>5</sup> Unfortunately, more than 10% of this dyestuff ends up in the environment as constituents of untreated or improperly treated effluents.<sup>6</sup> This is because when dyes are applied to fabric materials, not all the dye molecules are retained by the materials, and specific loss of dyes has been estimated to range between 2% and 50% for basic dye and reactive dyes, respectively.<sup>7</sup> In textile industries, the effluents could be in liquid or solid forms consisting of chelating agents, emulsifying oils, softening agents, surfactants, acids, promoting agents and dyes used in the dyeing process. Hence, the effluent is characterized by high pH, intense colour, suspended solids and dissolved solids.<sup>8</sup> Unfortunately, textile dyes in the effluent have been associated with many environmental and living organism problems. For instance, they prevent the growth of aquatic organisms and limit the self-purification of water.<sup>9,10</sup> Additionally, when humans and animals are exposed to water polluted with textile dyes, they face many health hazards. Thus, the negative impacts of water pollution by textile dyes are related to health, economic and environmental issues. Therefore, efficient and sustainable solutions must be provided to eliminate these textile dyes from polluted water.

Since textile dyes have been established to persist as non-biodegradable organics in the environment and traditional wastewater treatment options have proven ineffective, concerted efforts have been dedicated to developing novel methods capable of completely eliminating textile dyes from wastewater. Earlier researchers embraced the adsorption

<sup>a</sup>Department of Chemical Sciences, University of Johannesburg, Doornfontein, P.O. BOX 17011, 2028 Johannesburg, South Africa. E-mail: nmabuba@uj.ac.za

<sup>b</sup>Institute for Nanotechnology and Water Sustainability (iNanoWS), College of Science, Engineering and Technology, University of South Africa, Private Bag X6, Florida Science Campus, 1709 Johannesburg, South Africa



process as a simple and cost-effective method for the removal of dyes from wastewater, and they explored the use of several materials as suitable adsorbents. Examples of such adsorbents include metal oxide nanoparticles,<sup>11,12</sup> carbonaceous materials<sup>13</sup> and low-cost biosorbents derived from agricultural wastes.<sup>14,15</sup> Unfortunately, the adsorption process has reported limited success in this regard, and it also suffers the problem of the generation of secondary pollutants.<sup>16</sup> Recently, methods based on advanced oxidation processes (AOPs), which largely depend on the use of reactive oxygen species (ROS) such as hydroxyl radicals and superoxide radicals as powerful oxidants, have been identified to be capable of total removal of textile dyes from wastewater.<sup>17</sup> A prominent example of AOPs is the photocatalysis process which involves the use of metal oxide semiconductors such as TiO<sub>2</sub>,<sup>18</sup> ZnO,<sup>19</sup> BiVO<sub>4</sub>,<sup>20</sup> Bi<sub>2</sub>WO<sub>6</sub>,<sup>21</sup> Cu<sub>2</sub>O<sup>22</sup> and WO<sub>3</sub>.<sup>23</sup> However, the problems of rapid recombination of charge carriers limit the success of photocatalytic removal of textile dyes in wastewater. This led to the development of photoelectrocatalytic degradation process, whereby the application of bias potential significantly reduces the issue of spontaneous recombination of photogenerated charge carriers in the semiconductors.<sup>24</sup>

Tremendous success has been recorded in applying the photoelectrocatalysis (PEC) process for removing textile dyes from wastewater using various kinds of photoanodes. Hence, this review aims to present a critical discussion on the recent advancement in the use of a wide range of anodic materials to remove a commonly used textile dye, rhodamine B, in wastewater. It is worth noting that the removal of rhodamine B has been the subject of many research studies due to its unpleasant effects when found in water environments. In fact, the amount of literature available on the removal of rhodamine B has prompted many researchers to write review articles to understand the progress and intricacies of eliminating rhodamine B from wastewater. For example, Al-Gheethi *et al.* published a review on the removal of rhodamine B using adsorbents made from agricultural wastes.<sup>25</sup> In another recently published work by Al-Buriah *et al.*, a critical discussion on the use of nanoparticle photocatalysts for the removal of rhodamine B from textile wastewater was presented.<sup>26</sup> However, the focus of this review is on the use of PEC degradation technique for the removal of rhodamine B from wastewater. A robust discussion is presented on different novel materials that have been employed as photoanodes as well as their preparation. The factors affecting the PEC degradation processes were succinctly enumerated, along with the kinetics and mechanisms of the process. Hence, this review article will benefit scientists concerned with finding sustainable ways to remove organic dyes from polluted water.

## 2 Rhodamine B dye

Rhodamine B dye is a common water-soluble dye that is widely used in textile industries for dyeing wool fabrics. Additionally, in other industries such as paper, plastic, printing, biomedical and leather industries, rhodamine B is commonly employed as a colouring agent, photosensitizers, water tracer, fluorescent

markers for microscopic structural analysis and biological stain in biomedical research.<sup>27–29</sup> Hence, it is a common constituent of effluents emanating from these industries. Rhodamine B, one of the oldest synthetic dyes employed in food and fabric dyeing industries, is an amphoteric dye belonging to the broad class of xanthene dyes. It is one of the most environmentally benign xanthene basic dyes.<sup>25</sup> According to IUPAC nomenclature, rhodamine B is called *N*-[9-(*ortho*-carboxyphenyl)-6-(diethylamino)-3*H*-xanthen-3-ylidene] diethyl ammonium chloride. It has a molecular weight of 479.02 g mol<sup>-1</sup> and exhibits maximum absorbance at a wavelength of 554 nm.<sup>30</sup> It is a highly water-soluble basic red dye, and its dissolved form can readily be extracted using ethanol or butanol. Generally, the preparation of rhodamine B depends on the modification of amino groups of xanthene compounds *via* a route that connects the units to form a glycosidic bond.<sup>31</sup> The typical chemical structure of rhodamine B (C<sub>28</sub>H<sub>31</sub>ClN<sub>2</sub>O<sub>3</sub>) is shown in Fig. 1. In a neutral condition, the closed/nonfluorescent spiroactam form and the open/fluorescent form of rhodamine B exist in equilibrium. However, under basic conditions, the closed form, which is colourless, is favoured while the open form is favoured under acidic conditions.<sup>32</sup>

Due to its vast applications in many industries that discharge partially treated effluents into the environment, it is not surprising to find rhodamine B in the water environment. Unfortunately, the water pollution by rhodamine B has been linked to many environmental issues and health risks in humans and animals. Even when the concentration of rhodamine B in water is very low (approximately 1.0 mg L<sup>-1</sup>), it impacts a strong colour on the water, making it unsuitable for domestic use and consumption.<sup>33,34</sup> Aquatic organisms suffer greatly from the presence of rhodamine B in surface water as it significantly prevents the penetration of light to algae and other plants in the water, hindering the photosynthesis process. In a study conducted by Kooch *et al.*, it was observed that rhodamine B is hazardous to *Cyprinodon variegatus* at the lethal concentration of 84 mg L<sup>-1</sup>.<sup>35</sup> Additionally, in water contaminated by rhodamine B, it has been noted that the population of phytoplankton and zooplankton is very low.<sup>36</sup>

Furthermore, contact with rhodamine B can damage the eyes and cause irritation and severe oral noxiousness in humans.<sup>33</sup>

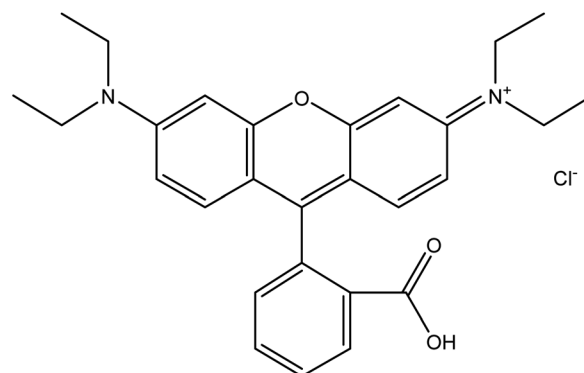


Fig. 1 Chemical structure of rhodamine B.



However, humans are susceptible to greater risks when they ingest rhodamine B. Studies in the field of medicine have confirmed that rhodamine B is mutagenic and carcinogenic in nature, causing developmental and simulation toxicity in animals and humans.<sup>37</sup> It has also been associated with the disruption of central nervous systems and other vital organs, including the liver, brain and kidney.<sup>38</sup> Hence, its use in food processing industries has been prohibited.<sup>39</sup> Nevertheless, it is paramount that effluents originating from industries dealing with rhodamine B are subjected to suitable wastewater treatment methods to absolutely remove rhodamine B from them before being discharged into the environment. This is very important since rhodamine B has reasonably good photostability<sup>40</sup> and hence cannot be easily degradable in the environment with exposure to direct sunlight.

In the quest to tackle the problem of water pollution due to the presence of rhodamine B dye, several wastewater treatment options have been explored for decolourisation and degradation of rhodamine B in water. These treatment options include processes based on physical, biological or chemical principles. A prominent example of these treatment options is the adsorption process which is very economical and environmentally friendly. This adsorption of rhodamine B has been ongoing for decades. In as much as it has its demerits, the research studies in this are still on the increase, and the choice of adsorbents is evolving. Recently, attention has been given to improving adsorption operation by incorporating membrane separation technology. For example, Wang *et al.* studied the removal of rhodamine B through an adsorptive membrane using a composite material consisting of graphene oxide–polydopamine coupled with polyethersulfone–sulfonated polyethersulfone membrane.<sup>41</sup> The adsorption process was found to be chemisorption, and an impressive adsorption capacity of 26.34 mg g<sup>-1</sup> was reported for the composite material. Similarly, in another study by Gharbani and Mehrizad, rhodamine B was removed through an adsorptive membrane process.<sup>42</sup> The material employed was a composite of graphitic carbon nitrides, chitosan and polyvinylidene fluoride. The maximum adsorption capacity for rhodamine B was reported to be 33.46 mg g<sup>-1</sup> which also corresponds to 72.74% removal of the dye. However, due to inherent limitations of the adsorption process, other wastewater treatment options particularly advanced oxidation processes.

Photocatalysis, an example of AOPs, has been extensively studied to remove rhodamine B in an aqueous solution. The process is also easy to operate and environmentally friendly. However, unlike the adsorption process, photocatalysis can completely mineralise rhodamine B molecules in aqueous solutions. Though numerous kinds of pristine metal oxides semiconductors have been employed for the photocatalytic removal of rhodamine B, the majority of the recent photocatalysts are composites of two or more metal oxides with heterojunctions. For example, Harish *et al.* reported the photocatalytic removal of rhodamine B dye using a binary composite of molybdenum disulfide and nickel disulfide (MoS<sub>2</sub>/NiS<sub>2</sub>).<sup>43</sup> The nanocomposite consisting of several spherical particles with nanosheets was prepared through the

hydrothermal method at a temperature of 180 °C for 24 h. When the composite material was applied for photocatalytic removal of rhodamine B under visible light illumination, the percentage degradation was found to be approximately 91%. In another study reported by Truong *et al.*, nanocomposite of ZnO and CuO was successfully applied for the photocatalytic degradation of rhodamine B.<sup>44</sup> The material was prepared using the sol-gel method followed by calcination. The material achieved 98% removal of rhodamine B through photocatalysis, and this was higher than the percentage recorded using pristine ZnO and CuO. Other composites that have been recently reported for the photocatalytic degradation of rhodamine B include ZnO/ZnFe<sub>2</sub>O<sub>4</sub>,<sup>45</sup> BiOI/MgCrO<sub>4</sub>,<sup>46</sup> ZnO/PbCrO<sub>4</sub> (ref. 47) and C<sub>3</sub>N<sub>4</sub>/CoWO<sub>4</sub>.<sup>48</sup>

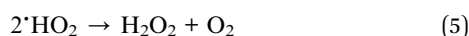
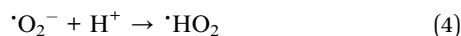
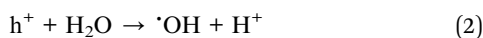
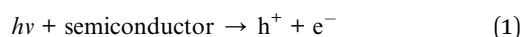
Another wastewater treatment option that has been employed for the removal of rhodamine B in water is the photo-Fenton process. This process is similar to classic Fenton, where H<sub>2</sub>O<sub>2</sub> and ferrous ions are used to produce hydroxyl radicals to oxidise organics.<sup>49</sup> However, unlike the typical Fenton process where ferrous salt is needed, in the photo-Fenton process, the semiconductor photocatalyst also serves as the source of the ferrous ion and a light source is also used. This strategy helps minimize the rapid recombination of photogenerated electron-hole pairs in the photocatalyst. In a study by Welter *et al.*, degradation of rhodamine B was achieved through a photo-Fenton process using a composite of chitin biochar and ZnFe<sub>2</sub>O<sub>4</sub>.<sup>50</sup> This material was prepared using the sol-gel method, and the presence of biochar in the composite promoted efficient charge separation in the ZnFe<sub>2</sub>O<sub>4</sub>. Impressively, after 1 h, 100% discolouration of rhodamine B was achieved in the photo-Fenton process. In another study by Zhang *et al.*, iron-copper-supported montmorillonite was used for the photo-Fenton removal of rhodamine B dye. A two-step strategy of impregnation and calcination was adopted for the preparation of the catalyst. After 90 min, 98% discolouration of rhodamine B was recorded using the material. Due to the great prospect of Fenton processes for degradation of organics, the electro-Fenton process has also been studied to remove rhodamine B dye.<sup>51,52</sup>

### 3 Photoelectrocatalytic degradation: fundamentals

Photoelectrocatalytic oxidation is an example of an advanced electrochemical oxidation process with applications in sensing, water splitting and degradation of organics. The foundation of PEC process can be traced to the pioneering work on photoelectrochemistry by Brattain and Garrett.<sup>53</sup> Later, the concept of water splitting in photoelectrochemistry was discovered by Fujishima and Honda in 1972 where they employed TiO<sub>2</sub> as the photoanode.<sup>54</sup> Generally, PEC process combines the photocatalytic process synergistically with electrochemical oxidation. Typically, in PEC degradation process, a photoactive material, usually a metal oxide semiconductor, is employed as the anode (photoanode) and then irradiated with light of suitable wavelength along with the passage of electrical energy through the



electrode.<sup>55</sup> When exposed to light, the photoanode absorbs photons and excites electrons from the semiconductor's valence band to its conduction band, much like in traditional heterogeneous photocatalysis. As a result, holes are formed, which are oxidants capable of degrading organic molecules in the solution. Additionally, the holes produce hydroxyl radicals from their interactions with water molecules at the anode surface. The hydroxyl radicals which are strong oxidants further oxidize the organic molecules to carbon dioxide, water molecules or lower chain hydrocarbons. Since this process in PEC system is similar to the mechanism of photocatalysis, it is expected that the issue of spontaneous recombination of photogenerated electron-hole pairs will limit the efficiency of the oxidation process. However, the application of external potential provides a force to drive away electrons from the photoanode resulting in the promotion of charge separation and reduction the in combination of photogenerated charge carriers.<sup>56</sup> It is also important to note that the electrons facilitate the formation of other oxidants within the PEC system. Specifically, apart from holes and hydroxyl radicals, other oxidizing species in PEC system include superoxide and hydroperoxyl radicals. Eqn (1)–(5) summarize the formation of these oxidants from the photoanode.<sup>55,57</sup>



Even though PEC degradation incorporates elements of photocatalysis and electrochemical oxidation, it has some outstanding advantages over the two processes. Though, unlike some AOPs, the PEC degradation process requires the use of electrical power sources like potentiostat which may be expensive and require special expertise, the desirable advantages of PEC process over other AOPs make the process attractive. In addition to efficient charge separation that is obtainable in PEC, it offers better and easy reusability of photoactive material than in photocatalysis. In photocatalysis, the powdered or granular photocatalysts often require regeneration with chemical reagents for reuse. However, in PEC degradation system, the photoactive materials constitute compact electrodes and hence can simply be rinsed with deionised water, dried and reused. This is more economical and time-efficient. Furthermore, when PEC system is compared with the electrochemical oxidation process (anodic oxidation), a prominent advantage is that lower bias potential is sufficient for the mineralisation of organics in PEC system, unlike anodic oxidation, which requires a higher magnitude of applied cell potential.<sup>58</sup>

In PEC degradation, the choice of the photoanode material plays a crucial role in achieving better efficiency. Like in photocatalysis, the semiconducting metal oxides that have been mostly explored as suitable photoactive materials for the anode

in PEC degradation systems are TiO<sub>2</sub> and ZnO.<sup>59–62</sup> These systems have been extensively adopted for the mineralisation of a wide range of organics, including pesticides, dyes, pharmaceuticals and phenolic compounds.<sup>63,64</sup> The major hindrance to using TiO<sub>2</sub> and ZnO as photoanodes is their relatively large band gap energies (~3.5 eV for TiO<sub>2</sub>) which dictate the use of UV irradiation for better excitation electrons.<sup>56</sup> However, humans are at risk when exposed to UV irradiation.

Additionally, the high cost associated with the use of TiO<sub>2</sub> and ZnO photoanodes due to the cost of UV light sources is a key demerit. Hence, researchers have explored numerous strategies to make TiO<sub>2</sub> and ZnO absorb photons within the visible light region as this will encourage the use of sunlight as the source of irradiation. Such strategies include tuning morphologies and doping with both non-metal and metal elements. For example, boron, nitrogen, graphene, nitrogen and fluorine are common non-metal dopants that have been used to promote visible light absorption in TiO<sub>2</sub>.<sup>65–67</sup>

In the last few years, the use of visible light-active metal oxide semiconductors as photoanode materials in PEC has been embraced. These materials have narrow band gaps and can easily absorb photons for excitation within the visible light spectrum, and their use encourages the adoption of direct sunlight as a suitable light source for PEC degradation systems. Examples of visible light active that are common as photoanodes for PEC degradation of organics include g-C<sub>3</sub>N<sub>4</sub>,<sup>68</sup> BiVO<sub>4</sub>,<sup>69</sup> WO<sub>3</sub>,<sup>70</sup> MoS<sub>2</sub>,<sup>71</sup> Bi<sub>2</sub>WO<sub>6</sub>,<sup>72</sup> and Ag<sub>3</sub>PO<sub>4</sub>.<sup>73</sup> These materials have also been used to improve the performances of TiO<sub>2</sub> and ZnO.<sup>74–76</sup> As a result of the narrow band gap energies of these visible-light active semiconductors, they are more susceptible to the spontaneous recombination of photogenerated electron-hole pairs, which could significantly decrease the efficiencies of their PEC systems and, therefore, their use in pristine form is not encouraged. In order to combat this challenge, doping strategy has been used.<sup>77,78</sup> However, the construction of semiconductor-semiconductor heterojunction has recorded more success in this regard. A heterojunction is formed when two semiconductors of unequal band gap combine in such a way that results in band alignment, which enables the separation of photogenerated holes to the valence band and electrons to the conduction band.<sup>79</sup> Numerous examples of heterostructured photoanodes consisting of at least one visible light-responsive semiconductor have been reported for the PEC degradation of organics in wastewater. Examples include BiVO<sub>4</sub>/WO<sub>3</sub>,<sup>80</sup> Fe<sub>2</sub>O<sub>3</sub>/Bi<sub>2</sub>WO<sub>6</sub>,<sup>81</sup> Cu<sub>2</sub>O/Fe<sub>2</sub>O<sub>3</sub> (ref. 82) and BiVO<sub>4</sub>/Ag<sub>2</sub>S.<sup>83</sup>

## 4 PEC degradation of rhodamine B

The successful degradation of rhodamine B dye has been achieved through PEC oxidation using different photoanodes. Some of these photoanodes consisted of pristine metal oxide semiconductors, while others were doped of composite with heterojunctions. For the composite materials, the PEC efficiency is often compared to the corresponding pristine materials. The conducting substrates often employed are fluorine-doped tin oxide glass (FTO), titanium sheet or exfoliated graphite.



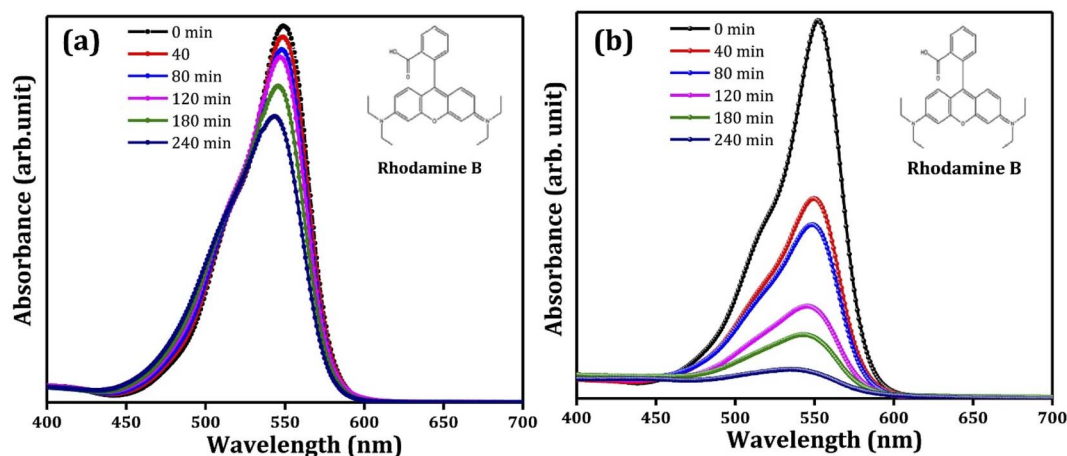


Fig. 2 Typical UV/visible spectra of removal of rhodamine B through (a) photocatalysis and (b) PEC degradation (reproduced from ref. 84 with permission from [Elsevier B.V.], copyright [2022]).

#### 4.1 Unmodified photoanodes

Pristine metal oxide semiconductors have been supported/immobilized on different conducting substrates for PEC degradation of rhodamine B. In a study conducted by Pedanekar *et al.*,  $\text{Bi}_2\text{WO}_6$  prepared on FTO glass was adopted as a suitable photoanode.<sup>84</sup> The photoanode was prepared by deposition of thin films of  $\text{Bi}_2\text{WO}_6$  on FTO glass through spray pyrolysis, and the volume of the spray solution was varied between 50 ml and 80 ml to obtain different  $\text{Bi}_2\text{WO}_6$ /FTO photoanodes. The prepared  $\text{Bi}_2\text{WO}_6$  has an orthorhombic crystal structure and a porous morphology consisting of several interconnected microparticles. The  $\text{Bi}_2\text{WO}_6$  electrode obtained with 70 ml spray solution showed better optical and electrochemical performances. The photoanode was then applied to degrade  $30 \text{ mg L}^{-1}$  rhodamine B dye solution under visible light irradiation with 0.7 V applied potential. After 2 h, 94% removal of rhodamine B was achieved. The degradation pattern as observed using UV-vis spectrophotometer are shown in Fig. 2(a and b). This percentage removal was over three times greater than the values obtained with photocatalysis and electrochemical oxidation using the same electrode. Additionally, the rate of degradation of the dye was fastest with PEC degradation. Similarly, in the works of Amaterz *et al.*, efficient degradation of rhodamine B was recorded using a photoanode made up of barium hydrogen phosphate films electrodeposited on FTO glass.<sup>85</sup> The PEC degradation of  $6.75 \text{ mol L}^{-1}$  of rhodamine B using the electrode resulted in 99% removal within just 7 min. In order to establish that the electrode achieves mineralisation of the dye and not just discolouration, the total organic carbon (TOC) value of the treated dye solution was measured, and an impressive value of 83% was recorded. The researchers also noted that coupling photocatalysis and electrocatalysis in the PEC degradation led to a synergistic effect in dye removal. These results clearly show that photoanodes consisting of pristine photoactive materials on FTO glass are capable of degrading rhodamine B molecules in PEC systems.

Furthermore, photoactive materials have also been prepared on titanium sheet or foil for the PEC removal of rhodamine B dye. For example, Zhou *et al.* reported the PEC removal of

rhodamine B dye using a photoanode consisting of  $\text{MoS}_2$  nanoflakes prepared on titanium foil.<sup>86</sup> The electrode was formed by growing  $\text{MoS}_2$  films on titanium foil in a Teflon-lined reactor through hydrothermal synthesis at  $180^\circ\text{C}$  for 24 h. Additionally, the  $\text{MoS}_2$  nanoflakes were further annealed at temperatures of  $300^\circ\text{C}$  and  $800^\circ\text{C}$ . The results from the XRD analysis revealed that the crystallinity of the  $\text{MoS}_2$  increased with an increase in annealing temperature. The  $\text{MoS}_2$  nanoplatelets were observed to be vertically aligned to the titanium foil, as shown in Fig. 3(a–f). The  $\text{MoS}_2$  PEC system was applied to remove rhodamine B dye with an initial concentration of  $1.0 \text{ mg L}^{-1}$ . After a 2 h reaction time with an applied potential of 0.5 V, the complete decolourisation of the rhodamine B dye solution was almost achieved. The primary oxidants in the  $\text{MoS}_2$  PEC system were found to be hydroxyl radicals as the degradation efficiency reduced significantly with the addition of *tert*-butyl alcohol. In a similar study conducted by the same group, it was observed that several reactive species such as superoxide radicals, oxysulfur radicals and hydroxyl radicals were produced in the  $\text{MoS}_2$  PEC system for degradation of rhodamine B.<sup>87</sup> The mechanism of this degradation process showing the generation of these radicals is depicted in Fig. 3g. In another study by Shao *et al.*,  $\text{Ru}_x\text{Zn}_{1-x}\text{O}$  was prepared on titanium plates and employed as a photoanode for PEC degradation of  $20 \text{ mg L}^{-1}$  rhodamine B dye solution.<sup>88</sup> Within 2 h, the percentage degradation of the dye was 97%, with an applied potential of 2.5 V. An attractive property of these electrodes prepared on titanium sheet or foil was that they offer excellent stability.

Though unmodified photoanodes have been identified as been capable of removal of rhodamine B through PEC oxidation, the efficiency of the process is significantly hindered as a result of rapid recombination of photogenerated electron–hole pairs. This problem can be overcome through appropriate modification of the material which may involve morphology control, doping and formation of heterojunction. These approaches seek to promote efficient charge separation in the photoanode which can then translate to improved PEC degradation efficiency. Another approach to counter the problem is



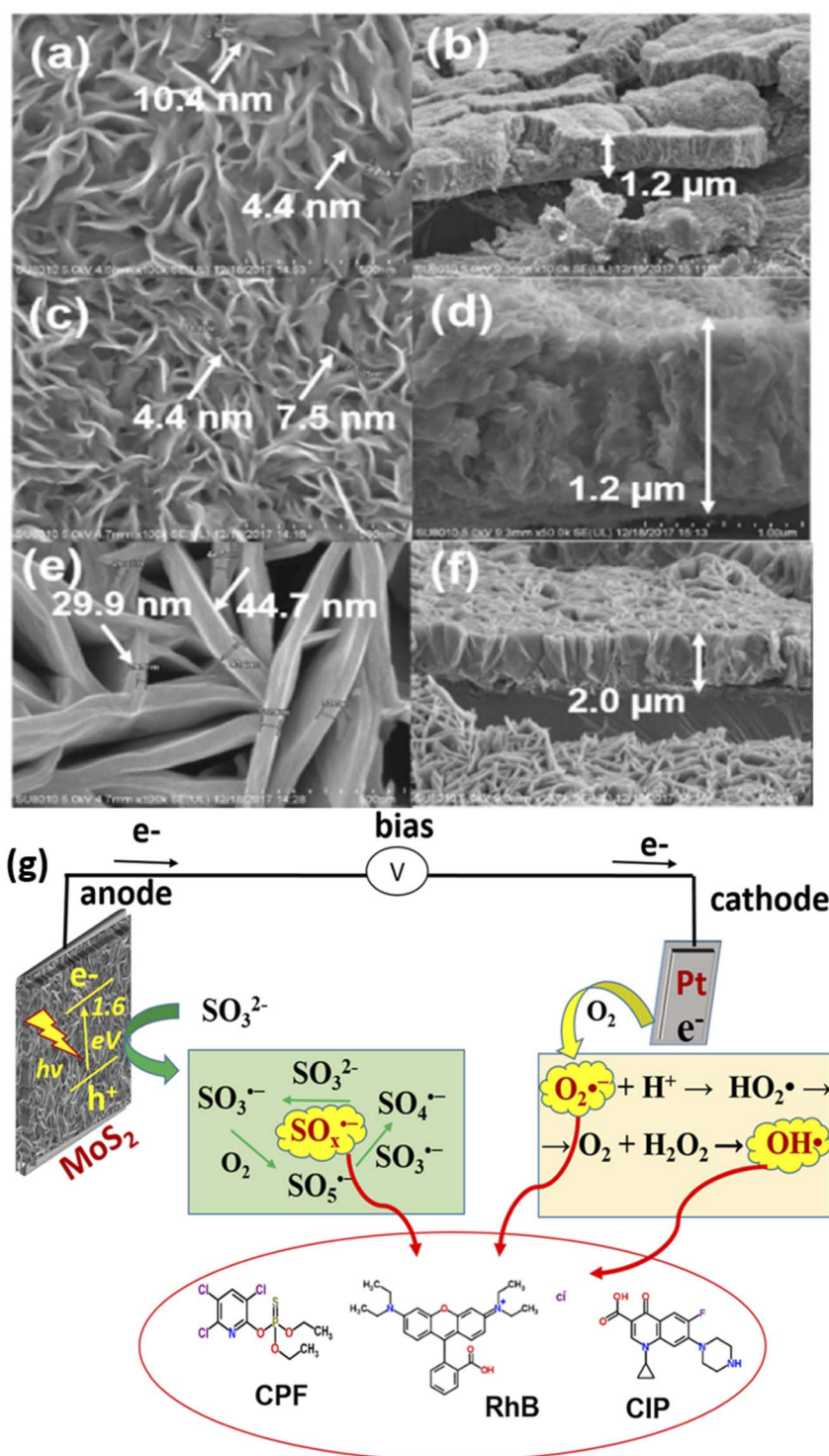


**Fig. 3** SEM images of as-prepared MoS<sub>2</sub> nanoflakes (a and b), MoS<sub>2</sub> (300 °C) nanoflakes (c and d) and MoS<sub>2</sub> (800 °C) (e and f) vertically aligned on Ti foil ((a, c and e) from top view; (b, d and f) from side view) (reproduced from ref. 86 with permission from [Elsevier B.V.], copyright [2022]) and illustration of PEC *in situ* generation of oxysulfur, superoxide and hydroxyl radicals (g) (reproduced from ref. 87 with permission from [IWA Publishing], copyright [2021]).

the choice of conducting substrate. For instance, exfoliated graphite can be employed because of its dual function of acting as electron sinking and being a good conductor. Titanium sheet can also be anodized to TiO<sub>2</sub> nanotubes which can form heterojunction with other metal oxide semiconductors.

#### 4.2 Doped photoanodes

In recent studies, modified photoanodes are often employed for PEC degradation of rhodamine B to overcome the problem of rapid recombination of photogenerated electron-hole pairs



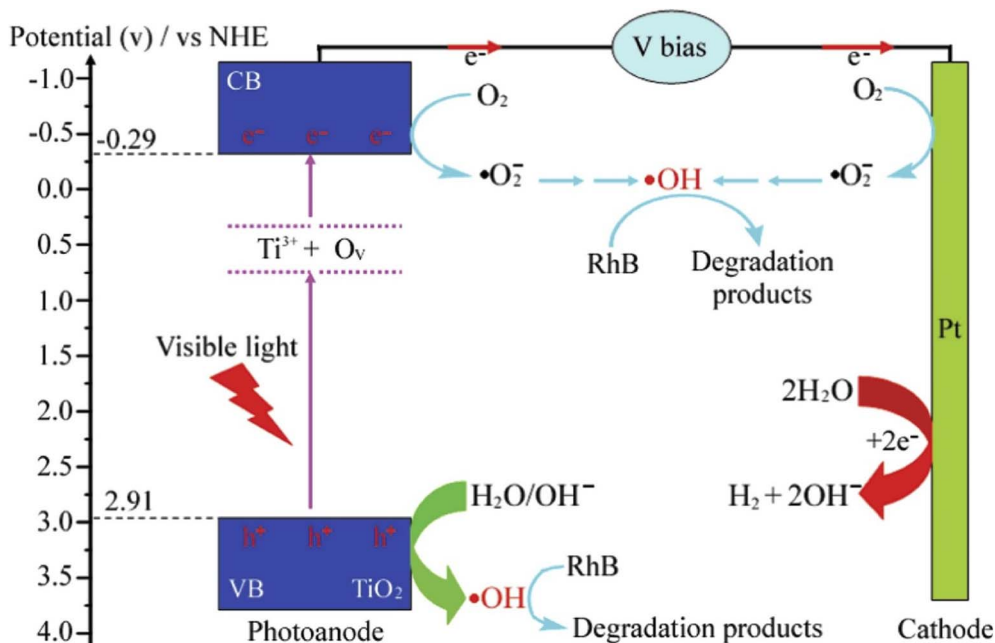


Fig. 4 Schematic diagram of PEC degradation of rhodamine B (RhB) using  $\text{Ti}^{3+}$  self doped  $\text{TiO}_2$  (reproduced from ref. 93 with permission from [Elsevier B.V.], copyright [2016]).

prevalent in pristine photoanodes or to increase the visible light responsiveness of the photoanodes. The doping of metal oxide semiconductors with metals and non-metals has proven to be an effective strategy to increase the PEC efficiency of photoanodes in the degradation process. When a dopant is introduced into the structure of semiconductors, it can shift the band edge towards the visible region, induce oxygen vacancy, induce carrier trap density and increase the mobility of the charge carriers. This results in improve conductivity and photosensitivity.<sup>89</sup> Many researchers have investigated the use of doped photoanodes for the PEC degradation of rhodamine B dye. For example, Reis *et al.* reported the use of nitrogen-doped ZnO as an ideal photoanode for PEC removal of rhodamine B.<sup>90</sup> The photoanode was prepared through electrodeposition of ZnO on FTO glass under continuous nitrogen gas bubbling at different rates. Though doping the ZnO with nitrogen did not cause a change in the band gap energy of the ZnO, it did increase both the optical and photoelectrochemical properties of the photoanode. As evidence, the photocurrent response of the nitrogen-doped ZnO was around  $70 \mu\text{A cm}^{-2}$  which was higher than of the pristine ZnO ( $48 \mu\text{A cm}^{-2}$ ). This was because doping with nitrogen promoted better electron mobility and reduced the electrical resistance of the ZnO. When the electrodes were applied for the PEC degradation of  $0.48 \text{ mg L}^{-1}$  rhodamine B solution, the catalytic efficiencies were 26% and 43% for pristine ZnO and nitrogen-doped ZnO electrodes, respectively. These findings confirmed that doping with non-metals such as nitrogen is an effective strategy to improve PEC efficiencies of photoanodes.

In the case of  $\text{TiO}_2$ , both metals and non-metals have been used as dopants to improve its PEC performance towards the mineralisation of rhodamine B dye. For example, Kiziltas

reported the PEC degradation of rhodamine B using a photoanode consisting of  $\text{TiO}_2$  nanotubes codoped with boron and cobalt.<sup>91</sup> The photoanode was prepared through anodization of titanium sheets in the presence of cobalt and boron salts, followed by calcination at  $500^\circ\text{C}$  for 2 h. The dopants significantly decreased the band gap energy of  $\text{TiO}_2$  which resulted in better light absorption. Additionally, the photocurrent density recorded for the codoped  $\text{TiO}_2$  nanotubes was  $2.1 \text{ mA cm}^{-2}$  with applied potential of 0.6 V, which was almost seven times higher than the response of pristine  $\text{TiO}_2$  nanotubes ( $0.31 \text{ mA cm}^{-2}$ ). The codoped photoanode achieved 95.5% PEC removal of  $10 \text{ mg L}^{-1}$  rhodamine B solution within 90 min while the undoped  $\text{TiO}_2$  nanotube degraded only 46.3% of the dye. This result evidently revealed that binary doping of photoanode can improve the PEC efficiency of the photoanode through enhanced electron mobility and better photon absorption. Selenium is another metal that has been employed as dopant for  $\text{TiO}_2$  nanotubes towards PEC degradation of rhodamine B.<sup>92</sup> The selenium doped  $\text{TiO}_2$  achieved approximately 73% PEC removal of the dye while only 28% removal was recorded with the undoped material. The enhanced PEC performance was attributed improved visible light absorption due to the incorporation of selenium. Interestingly, self-doping approach with  $\text{Ti}^{3+}$  is another ideal way to extend the light responsiveness of  $\text{TiO}_2$ . Wu *et al.* reported 10% and 99.9% PEC removal of rhodamine B within 50 min using undoped  $\text{TiO}_2$  and  $\text{Ti}^{3+}$  doped  $\text{TiO}_2$  photoanodes, respectively.<sup>93</sup> The superior performance was linked to faster transport of photogenerated charge carriers, reduced recombination rate and improved light absorption due to  $\text{Ti}^{3+}$  self doping. As shown in Fig. 4, it can be seen that the  $\text{Ti}^{3+}$  introduced local states between the valence band and conduction band of  $\text{TiO}_2$  which enlarged the optical



absorption of photoanode. Hence, doping photoanodes with metals is an effective method of improving PEC degradation of rhodamine B dye.

Nurdin *et al.* also reported the PEC degradation of rhodamine B using a TiO<sub>2</sub> electrode codoped with both metal and non-metal dopants.<sup>94</sup> In their study, manganese and nitrogen were employed as suitable dopants to improve the performance of TiO<sub>2</sub>. A sol-gel method was employed to successfully dope the TiO<sub>2</sub> films on a titanium sheet with the elements. The codoped TiO<sub>2</sub> electrode showed better PEC efficiency under visible light illumination. Interestingly, the codoped electrode achieved 74.2% PEC removal of 0.5 mg L<sup>-1</sup> rhodamine B dye under visible light illumination, whereas the best performance of the undoped TiO<sub>2</sub> electrode under UV irradiation was 63%. Hence, doping with both manganese and nitrogen increased the visible light absorption of TiO<sub>2</sub> by reducing the charge recombination and improving electron mobility. The mechanism of charge separation within the codoped electrode and the degradation of the dye molecules are depicted in Fig. 5. Such impressive PEC degradation of rhodamine B using TiO<sub>2</sub> photoanode doped with both metal and non-metal dopants was also observed in the study reported by Kothavale *et al.*, where boron and nitrogen were used as the dopants.<sup>95</sup>

Considering the reports on the use of doped photoanodes for the removal of rhodamine B dye in aqueous solution through PEC oxidation, it can be inferred that numerous kinds of dopants can be adopted to improve the efficiency of the process. These dopants could be non-metals or metals which can easily extend the range of visible light absorbance of the photoanodes and also facilitate efficient charge separation within the photoanode. Hence, doped photoanodes offer better performance than undoped photoanodes. However, the choice of appropriate

dopants and optimization of the doping process are very important to achieve a photoanode with good PEC efficiency.

### 4.3 Heterostructured photoanodes

Several types of photoanodes with semiconductor-semiconductor heterojunctions have been employed for the PEC degradation of rhodamine B dye in aqueous solutions. The use of heterostructured photoanode is attractive because they offer better efficiencies due to improve charge separations. The heterostructured photoanode may consist of p-n heterojunction or n-n heterojunction depending on the type of semiconductors used. For example, Jiang *et al.* reported the use of Bi<sub>2</sub>O<sub>3</sub>/WO<sub>3</sub> photoanode with p-n heterojunction for the PEC degradation of rhodamine B dye.<sup>96</sup> The composite films were prepared through hydrothermal synthesis onto FTO glass at a temperature of 160 °C for 6 h followed by calcination at 600 °C for 2 h. The optical characterisation results showed that heterojunction formation led to an increase in the absorption of visible light by the Bi<sub>2</sub>O<sub>3</sub>/WO<sub>3</sub>. Additionally, the composites photoluminescence intensity was weaker than the pristine Bi<sub>2</sub>O<sub>3</sub> and WO<sub>3</sub>, which suggested a decrease in the recombination of charge carriers. The measurement of photocurrent responses further confirmed the improved charge separation in the Bi<sub>2</sub>O<sub>3</sub>/WO<sub>3</sub> interface due to the formation of p-n heterojunction. Consequently, when the photoanodes were applied for the PEC degradation of 10 mg L<sup>-1</sup>, the highest removal efficiency (73.4%) was recorded with the Bi<sub>2</sub>O<sub>3</sub>/WO<sub>3</sub> photoanode, which Bi<sub>2</sub>O<sub>3</sub> and WO<sub>3</sub> gave 33.3% and 25.9% respectively after 3 h. Hence the construction of p-n heterojunction with effective charge separation could effectively increase the PEC efficiency of removal of rhodamine B dye.

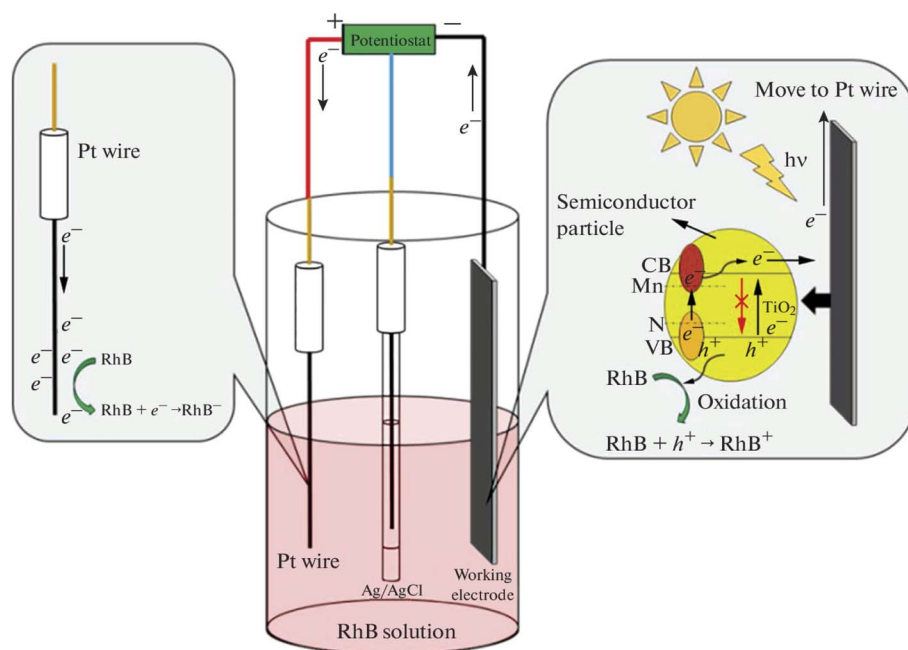


Fig. 5 Presentation of PEC system for rhodamine B dye degradation at Mn, N doped TiO<sub>2</sub> electrode (reproduced from ref. 94 with permission from [Allerton Press, Inc.], copyright [2022]).



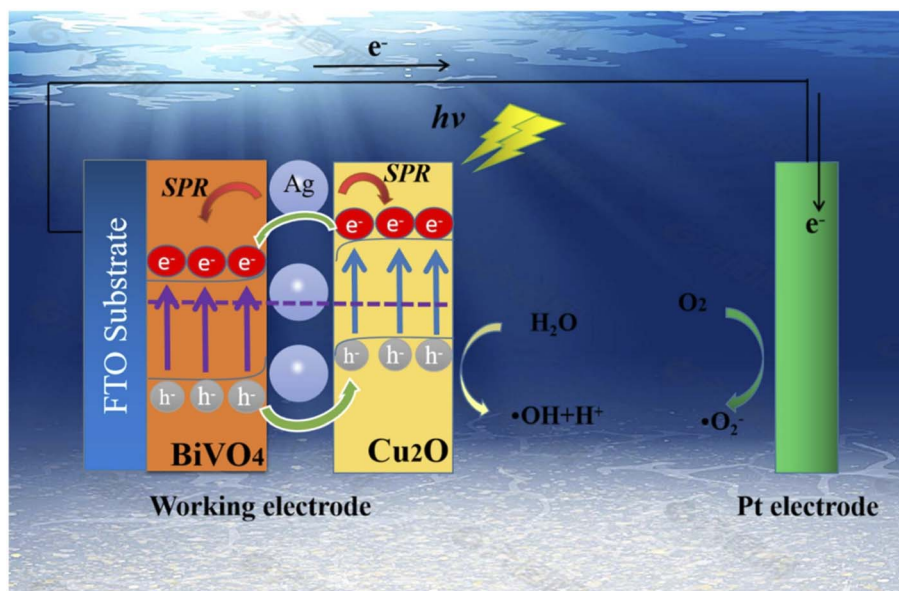


Fig. 6 Schematic diagram illustrating the enhanced charge separation in Ag/BiVO<sub>4</sub>/Cu<sub>2</sub>O photoanodes in the PEC degradation of rhodamine B (reproduced from ref. 97 with permission from [Elsevier B.V.], copyright [2022]).

In another study by Ma *et al.*, a composite photoanode of BiVO<sub>4</sub>/Cu<sub>2</sub>O with p–n heterojunction decorated with silver nanoparticles was employed for the PEC degradation of rhodamine B.<sup>97</sup> The BiVO<sub>4</sub> was firstly prepared on FTO glass through hydrothermal synthesis, and silver nanoparticles were then deposited on it by a facile chemical water bath method. To obtain the p–n heterojunction, Cu<sub>2</sub>O were electrodeposited onto the prepared BiVO<sub>4</sub>/Ag/FTO at a potential of  $-0.5$  V for 3 min. The morphology of the composite revealed that the photoanode consisted of compact BiVO<sub>4</sub> nanosheets and Cu<sub>2</sub>O cubic nanocubes, which were agglomerated with Ag nanoparticles. The prepared BiVO<sub>4</sub>/Cu<sub>2</sub>O showed an improved response to visible light because of better charge separation through the formation of p–n heterojunction as shown in Fig. 6. Specifically, the absorption band edge of BiVO<sub>4</sub> shifted from 512 nm to 549 nm in the BiVO<sub>4</sub>/Cu<sub>2</sub>O. The addition of Ag nanoparticles increased it to 568 nm due to the plasmon resonance effect. The percentage PEC removals of 5 mg L<sup>-1</sup> rhodamine B with an applied potential of 1.2 V under visible light after 2 h were 30%, 69% and 86% using BiVO<sub>4</sub>, BiVO<sub>4</sub>/Cu<sub>2</sub>O and Ag/BiVO<sub>4</sub>/Cu<sub>2</sub>O photoanodes, respectively. The better removal achieved in the composite electrode was attributed to the resultant effect of enhanced charge separation and plasmon resonance effect. This further proved the suitability of p–n heterostructured photoanodes for removal of rhodamine B.

Improved PEC degradation of rhodamine B dye has also been achieved using photoanodes consisting of n–n heterojunction. Davaslioglu *et al.* report that a photoanode made up of WO<sub>3</sub> and TiO<sub>2</sub> nanotubes with n–n heterojunction were used for the PEC degradation of rhodamine B.<sup>98</sup> The composite electrode was fabricated by electrodeposition of WO<sub>3</sub> onto TiO<sub>2</sub> nanotube arrays. As shown in Fig. 7(a and b), formation of heterojunction resulted in lower electric resistance and higher photocurrent responses. This was because the recombination of the

photogenerated electron–hole was significantly reduced as the charge carriers were separated through the formation of heterojunction. Consequently, the heterostructured photoanode achieved about 70% PEC removal of rhodamine B within 30 min. This value was significantly higher than the performance of pristine TiO<sub>2</sub> nanotubes suggesting that the formation of heterojunction is an effective way of increasing the PEC efficiencies of photoanodes. In another work by Orimolade *et al.*, a composite electrode consisting of BiVO<sub>4</sub>/ZnO with n–n heterojunction achieved 91% removal of rhodamine B through PEC process.<sup>99</sup> The mechanism of the degradation process, as shown in Fig. 7c, revealed that band alignment between BiVO<sub>4</sub> and ZnO resulted in the separation of photogenerated holes from the valence band of ZnO into that of BiVO<sub>4</sub>, which facilitated enhanced production of hydroxyl radicals resulting in better mineralisation of rhodamine B dye. Therefore, photoanodes with n–n heterojunctions are also ideal for the degradation of rhodamine B dye in an aqueous solution. It is also worth noting that the use of exfoliated graphite contributed to the efficiency of the system by serving as electron sink which enhanced photogenerated charge separation.

Evidently, heterostructured photoanodes have demonstrated better efficiencies in the PEC degradation of rhodamine B as compared to the use of pristine photoanodes. It is not surprising that many recent works are very particular about the fabrication of novel heterostructured photoanodes for PEC degradation of rhodamine B dyes and other organic pollutants. Though, doped photoanode have also recorded higher performance than undoped photoanode, the use of heterostructured is much attractive because of the possibility of coupling the strengths of two or more metal oxides semiconductors. For instance, a visible light active semiconductor can be used to improve the visible light responsiveness of UV active semiconductors. Additionally, improved charge separation is often



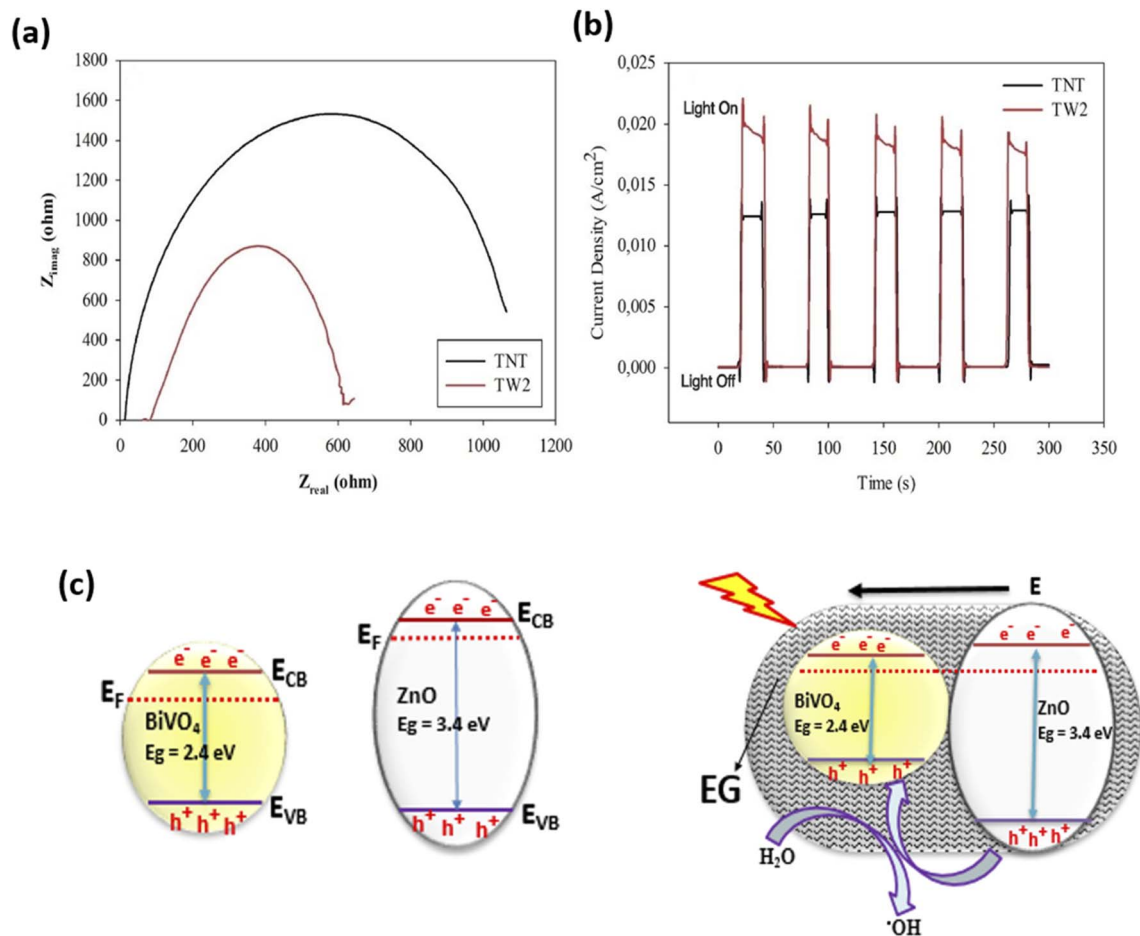


Fig. 7 Nyquist plots for pristine  $\text{TiO}_2$  nanotubes (TNT) and  $\text{WO}_3$  deposited  $\text{TiO}_2$  electrode (TW2) (a); Transient photocurrent response of bare  $\text{TiO}_2$  and  $\text{WO}_3$  deposited  $\text{TiO}_2$  electrode (b) (reproduced from ref. 98 with permission from [Elsevier B.V.], copyright [2021]) and Mechanism of charge separation in  $\text{BiVO}_4/\text{ZnO}$  n-n heterojunction (c) (reproduced from ref. 76 with permission from [Royal Society of Chemistry], copyright [2019]).

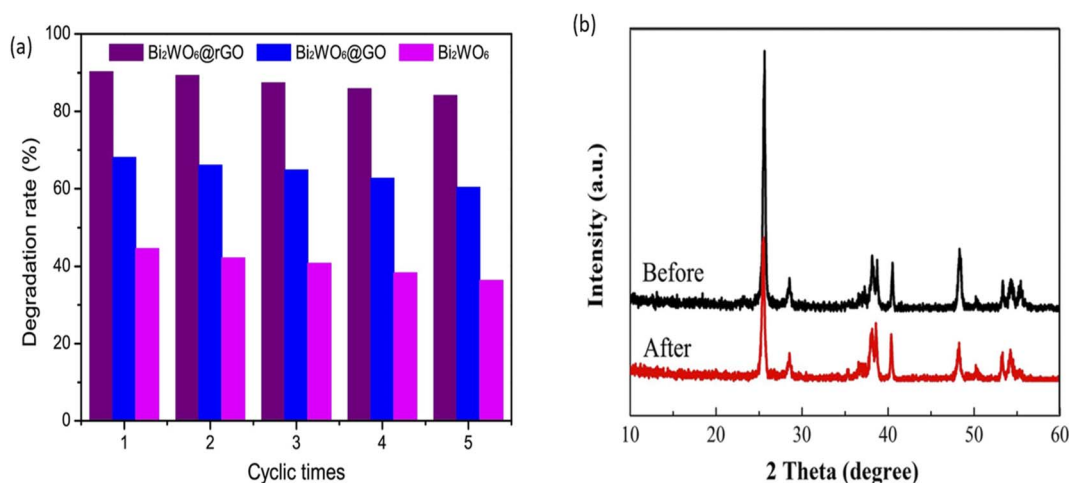


Fig. 8 Reusability test for PEC degradation of rhodamine B using  $\text{Bi}_2\text{WO}_6/\text{rGO}$  (a) (reproduced from ref. 100 with permission from [Elsevier B.V.], copyright [2017]) and XRD spectra of  $\text{Bi}_2\text{WO}_6/\text{TiO}_2$  before and after PEC degradation of rhodamine B (b) (reproduced from ref. 101 with permission from [Elsevier B.V.], copyright [2018]).



Table 1 Summary of recent studies on PEC degradation of rhodamine B

| Photoanode   | Synthesis                  | PEC condition   | Light source                | Conc                   | % removal           | Rate constant                           | Ref. |
|--|----------------------------|---|-----------------------------|------------------------|---------------------|---|------|
| <b>Unmodified photoanodes</b>                        |                            |   |                             |                        |                     |   |      |
| Bi <sub>2</sub> WO <sub>6</sub> /FTO                 | Spray pyrolysis            | Potential: 0.7 V vs. SCE<br>Pt wire and SCE as counter and reference electrode respectively                     | 500 W tungsten filament     | 30 mg L <sup>-1</sup>  | 94% after 4 h       | 1.08 × 10 <sup>-4</sup> s <sup>-1</sup> | 84   |
| Bi <sub>2</sub> S <sub>3</sub> /FTO                  | Radio frequency sputtering | Potential: 1.0 V vs. Ag/AgCl<br>Pt wire and Ag/AgCl as counter and reference electrode respectively             | 100 W xenon lamp            | 10 <sup>-5</sup> M     | 89.2% after 80 min  | 0.0204 min <sup>-1</sup>                | 102  |
| MoS <sub>2</sub> /Ti                                 | Hydrothermal               | Potential: 0.5 V<br>Pt foil and Ag/AgCl as counter and reference electrode respectively                         | 300 W xenon lamp            | 1 mg L <sup>-1</sup>   | 100% after 2 h      | 0.00936 min <sup>-1</sup>               | 86   |
| BaHPO <sub>4</sub> /FTO                              | Electrodeposition          | Current density: 13 mA cm <sup>-2</sup><br>Graphite rod and SCE as counter and reference electrode respectively | 250 W xenon lamp            | 6.75 M                 | 99% after 7 min     | —                                       | 85   |
| SrHPO <sub>4</sub> /FTO                              | Electrodeposition          | Current density: 10 mA cm <sup>-2</sup><br>Graphite rod and SCE as counter and reference electrode respectively | 250 W xenon lamp            | 10 mg L <sup>-1</sup>  | 94.5% after 12 min  | —                                       | 103  |
| MoS <sub>2</sub> /Ti                                 | Hydrothermal               | Potential: 0.3 V vs. Ag/AgCl<br>Pt foil and Ag/AgCl as counter and reference electrode respectively             | 300 W xenon lamp            | 2 μM                   | 100% after 4 h      | 0.0259 min <sup>-1</sup>                | 87   |
| Ru <sub>x</sub> Zn <sub>1-x</sub> O/Ti               | Thermal decomposition      | Potential: 2.5 V vs. SCE<br>Ti wire and SCE as counter and reference electrode respectively                     | —                           | 20 mg L <sup>-1</sup>  | 97% after 2 h       | —                                       | 88   |
| ZnO/FTO  | Electrodeposition          | Pt wire and SCE as counter and reference electrode respectively<br>Potential: 0.3 V                             | 7 W UV lamp                 | 10 mg L <sup>-1</sup>  | 99.98% after 30 min | 0.2155 min <sup>-1</sup>                | 104  |
| Zn <sub>3</sub> (PO <sub>4</sub> ) <sub>2</sub> /FTO | Electrodeposition          | Current density: -1 mA cm <sup>-2</sup><br>Graphite rod cathode   | 250 W xenon lamp            | 10 mg L <sup>-1</sup>  | 99% after 30 min    | —                                       | 105  |
| <b>Doped photoanodes</b>                             |                            |   |                             |                        |                     |   |      |
| B-Co/TiO <sub>2</sub>                                | Anodisation                | Potential: 0.6 V<br>Pt foil and Ag/AgCl as counter and reference electrode respectively                         | 254 nm W UV lamp            | 10 mg L <sup>-1</sup>  | 95.5% after 90 min  | —                                       | 91   |
| Mn-N/TiO <sub>2</sub> /Ti                            | Thermal oxidation          | Potential: 0.5 V<br>Pt foil and Ag/AgCl as counter and reference electrode respectively                         | —                           | 0.5 mg L <sup>-1</sup> | 74.2% after 60 min  | 0.0229 min <sup>-1</sup>                | 94   |
| N-ZnO/FTO  | Electrodeposition          | Potential: 0.7 V<br>Pt foil and Ag/AgCl as counter and reference electrode respectively                         | 150 W lamp                  | 1 μM                   | 43% after 160 min   | 0.023 min <sup>-1</sup>                 | 90   |
| N-TiO <sub>2</sub> /FTO                              | Chemical spray pyrolysis   | Potential: 0.5 V<br>Graphite cathode  | 20 W UV lamp                | 0.5 mM                 | 64% after 4 h       | —                                       | 95   |
| N-TiO <sub>2</sub>                                   | Ion implantation           | Pt mesh cathode<br>Potential: 2 V   | 300 W tungsten-halogen lamp | 80 mg L <sup>-1</sup>  | 43.2% after 80 min  | 0.011 min <sup>-1</sup>                 | 106  |
| C-TiO <sub>2</sub>                                   | Solvothermal               | Stainless steel as cathode  | —                           | 10 mg L <sup>-1</sup>  | 37.8% after 70 min  | —                                       | 107  |
| ZnO/Ag   | Chemical bath deposition   | Ag rod as counter electrode<br>Potential: 0.4 V   | 300 W Hg lamp               | 5 mg L <sup>-1</sup>   | 38% after 5 h       | —                                       | 108  |



Table 1 (Contd.)

| Photoanode   | Synthesis                     | PEC condition   | Light source       | Conc                  | % removal           | Rate constant                           | Ref. |
|--|-------------------------------|---|--------------------|-----------------------|---------------------|---|------|
| <b>Heterostructured photoanodes</b>                                |                               |   |                    |                       |                     |   |      |
| ZnFe <sub>2</sub> O <sub>4</sub> /TiO <sub>2</sub> /graphite       | Sol-gel                       | Pt plate as cathode<br>Potential: 15 V  | 500 W xenon lamp   | 20 mg L <sup>-1</sup> | 99% after 30 min    | 0.278 min <sup>-1</sup>                 | 109  |
| Ag <sub>3</sub> PO <sub>4</sub> /CNTs/Ni                           | Electrodeposition             | Pt foil and SCE as counter and reference electrode respectively<br>Potential: -0.1 V    | 500 W xenon lamp   | 5 mg L <sup>-1</sup>  | 95.44% after 12 min | —                                       | 110  |
| WO <sub>3</sub> /TiO <sub>2</sub> /FTO                             | Spray pyrolysis               | —   | Direct sunlight    | 1 mM                  | 58.7% after 160 min | 5.48 × 10 <sup>-7</sup> s <sup>-1</sup> | 111  |
| Bi <sub>2</sub> WO <sub>6</sub> @GO/ITO                            | Hydrothermal                  | Pt wire and SCE as counter and reference electrode respectively<br>Potential: 1 V       | 500 W xenon lamp   | 5 mg L <sup>-1</sup>  | 90% after 4 h       | —                                       | 100  |
| Bi <sub>2</sub> WO <sub>6</sub> /WO <sub>3</sub> /TiO <sub>2</sub> | Hydrothermal                  | Pt foil and Ag/AgCl as counter and reference electrode respectively<br>Potential: 1 V   | 500 W xenon lamp   | 5 mg L <sup>-1</sup>  | 66.07% after 2 h    | —                                       | 101  |
| Cu <sub>2</sub> O/TiO <sub>2</sub>                                 | SILAR                         | Pt foil and Ag/AgCl as counter and reference electrode respectively<br>Potential: 1 V   | 500 W xenon lamp   | 5 mg L <sup>-1</sup>  | 78% after 3 h       | —                                       | 112  |
| BiVO <sub>4</sub> /TiO <sub>2</sub>                                | Hydrothermal                  | Pt wire and Ag/AgCl as counter and reference electrode respectively<br>Potential: 6 V   | 300 W xenon lamp   | 10 mg L <sup>-1</sup> | 93.9% after 5 h     | —                                       | 113  |
| TiO <sub>2</sub> /Bi <sub>2</sub> MoO <sub>6</sub>                 | Solvothermal                  | Pt as counter electrode<br>Potential: 1 V   | 500 W xenon lamp   | 20 mM                 | 75% after 3 h       | 0.077 min <sup>-1</sup>                 | 114  |
| Bi <sub>2</sub> O <sub>3</sub> /WO <sub>3</sub>                    | Hydrothermal                  | Pt foil and SCE as counter and reference electrode respectively<br>Potential: 1 V       | 300 W xenon lamp   | 10 mg L <sup>-1</sup> | 73.5% after 3 h     | 0.0073 min <sup>-1</sup>                | 115  |
| GO/Ag <sub>3</sub> PO <sub>4</sub> /Ni                             | Electrodeposition             | Pt foil and SCE as counter and reference electrode respectively<br>Potential: 0.3 V     | —                  | 8 mg L <sup>-1</sup>  | 97.01% after 12 min | —                                       | 116  |
| rGO/BiOI/rGO   | Electrodeposition             | Pt wire and SCE as counter and reference electrode respectively<br>Potential: 1 V       | 300 W xenon lamp   | 5 mg L <sup>-1</sup>  | 80% after 5 h       | 0.322 h <sup>-1</sup>                   | 117  |
| BiVO <sub>4</sub> /WO <sub>3</sub>                                 | Dip coating                   | Pt wire and Ag/AgCl as counter and reference electrode respectively<br>Potential: 2 V   | 500 W xenon lamp   | 5 mg L <sup>-1</sup>  | 94% after 3 h       | —                                       | 118  |
| ZnO/CuWO <sub>4</sub> /FTO   | Hydrothermal                  | Pt wire and Ag/AgCl as counter and reference electrode respectively<br>Potential: 0.7 V | 150 W mercury lamp | 1 μM                  | 82% after 3 h       | 0.0078 min <sup>-1</sup>                | 119  |
| Bi <sub>2</sub> MoO <sub>6</sub> /WO <sub>3</sub>                  | Hydrothermal and solvothermal | Pt foil and SCE as counter and reference electrode respectively<br>Potential: 1.5 V     | 300 W xenon lamp   | 10 mg L <sup>-1</sup> | 80.1% after 4 h     | 0.0069 min <sup>-1</sup>                | 120  |
| ZnO/ZnS/FTO  | Hydrothermal                  | Pt wire and Ag/AgCl as counter and reference electrode respectively<br>Potential: 0.5 V | 100 W xenon lamp   | 0.1 mM                | 58% after 30 min    | 0.0249 min <sup>-1</sup>                | 121  |

accomplished with the formation of heterojunctions. It is therefore expected that more novel photoanodes for PEC degradation of rhodamine would still be investigated in the near future.

#### 4.4 Stability of photoanodes in PEC degradation of rhodamine B

An ideal photoanode for PEC degradation should possess good stability and reusability as this will project its potential for real-



life applications. In order to assess the stability and reusability of photoanodes, structural and morphology characterisations of the photoanode before and after use can be done to check for any changes resulting from leaching of the material into solution. Additionally, comparison of percentage removal of the dye after several use of the same photoanode is a suitable method to establish the extent of reusability of the photoanode. A good number of proposed photoanodes for removal of rhodamine has demonstrated good stability and reusability. For example, in the PEC degradation of rhodamine B using a composite photoanode consisting of  $\text{Bi}_2\text{WO}_6$  with reduced graphene oxide core shell ( $\text{Bi}_2\text{WO}_6@\text{GO}$ ), the photoanode displayed good reusability after five runnings.<sup>100</sup> As shown in Fig. 8, the change in the percentage removal after the fifth cycle was approximately 6% which confirmed that the electrode was stable. Likewise,  $\text{TiO}_2/\text{Bi}_2\text{WO}_6$  showed good stability in the PEC removal of rhodamine B which was affirmed from the XRD pattern of the photoanode after use. According to Fig. 8b, all the characteristic peaks of the material were still present after the use which suggested that electrode was stable.<sup>101</sup> Though many reports on the stability of photoanodes in PEC degradation adopted the approach of assessing the change in the PEC efficiency after several use, it would be better if researchers also subject the solution to analysis such as Inductively Coupled Plasma Optical Emission Spectroscopy (ICP-OES) to further check the leaching of the electrode into solution.

## 5 Summary and future perspectives

Photoelectrocatalytic degradation has remained an efficient treatment option for the degradation of organics in wastewater. The process is environmentally benign and cost-effective. As summarized in Table 1, much effort has been channelled towards removing rhodamine B dye from an aqueous solution. The results obtained are quite fascinating and impressive. Obviously, different kinds of metal oxide semiconductors can be employed as photoanodes for the PEC system involving rhodamine B. However, the use of visible light-responsive photocatalysts is more enticing because they offer better PEC efficiency with reduced cost due to the use of simulated solar irradiation or direct sunlight.

Nevertheless, most reported photoanodes for the removal of rhodamine B are modified either through doping or composite of two or more semiconductors with heterojunction. This is because photocatalysts are employed in their pristine form as photoanodes; they are more susceptible to spontaneous recombination of photogenerated electron-hole pairs, which tremendously reduces their PEC efficiency. Whereas, when modified appropriately, this problem can be circumvented through the promotion of efficient charge separation due to the formation of heterojunction or modification of band edge positions when doped, which results in higher PEC degradation efficiency of the dye. It is also very impressive to note that in some of the studies discussed, substantial removal of rhodamine B was achieved within a few minutes even with low applied potential, which confirmed the feasibility of adopting PEC oxidation for the treatment of textile effluents.

Nevertheless, there are some major issues that need to be addressed in future studies towards adopting PEC treatment for real-life applications. Firstly, in many of the reported work, the researchers did not report actual mineralisation of the rhodamine B molecule through total organic carbon (TOC) or determination of intermediate products. It is important to note that some of these intermediates could be more toxic than the parent rhodamine B molecules which necessitate conducting toxicity tests using bacteria strains. In addition to the toxicity of the intermediate products that can be challenging, formation of intermediate products could also increase the energy consumption of the PEC process. Computation of energy consumption within the process using the TOC values could provide appropriate insights on this.

Secondly, it is also troubling to note that the full experimental setup was not probably described in these studies, which makes it difficult for fair comparisons with other literature. In future studies, full description of the experimental setup is recommended. This should include the type of reactor use, the intensity of the light source, pollutant concentration, volume of working solution, the applied potential, distance of the photoanode from light source and other essential parameters that will facilitate easy reproducibility of the results and fair comparison with existing literature.

Additionally, the majority of the studies were conducted using simulated rhodamine B contaminated water but not real industrial effluent. Hence, it is recommended that future researchers pay more attention to the determination of the rate of mineralisation of rhodamine B and not just discoloration. Also, particular efforts should be directed to using real effluents for degradation studies. Overall, the PEC oxidation process has shown remarkable potential towards the treatment of wastewater laden with organic dyes such as rhodamine B.

## Conflicts of interest

There are no conflicts to declare.

## Acknowledgements

Dr T. L. Yusuf is grateful to the Faculty of Science, the University of Johannesburg, for a postdoctoral research fellowship award.

## References

- 1 C. Wu, C. Maurer, Y. Wang, S. Xue and D. L. Davis, *Environ. Health Perspect.*, 1999, **107**, 251–256.
- 2 P. Amoatey and M. S. Baawain, *Water Environ. Res.*, 2019, **91**, 1272–1287.
- 3 C. Zamora-Ledezma, D. Negrete-Bolagay, F. Figueroa, E. Zamora-Ledezma, M. Ni, F. Alexis and V. H. Guerrero, *Environ. Technol. Innovation*, 2021, **22**, 101504.
- 4 I. Som, M. Roy and R. Saha, *ChemCatChem*, 2020, **12**, 3409–3433.
- 5 M. A. Hassaan and A. El Nemr, *American Journal of Environmental Science and Engineering*, 2017, **1**, 64–67.



- 6 V. V. Chandanshive, S. K. Kadam, R. V. Khandare, M. B. Kurade, B. H. Jeon, J. P. Jadhav and S. P. Govindwar, *Chemosphere*, 2018, **210**, 968–976.
- 7 H. Ali, *Water, Air, Soil Pollut.*, 2010, **213**, 251–273.
- 8 D. A. Yaseen and M. Scholz, *Int. J. Environ. Sci. Technol.*, 2019, **16**, 1193–1226.
- 9 B. Lellis, C. Z. Fávaro-Polonio, J. A. Pamphile and J. C. Polonio, *Biotechnology Research and Innovation*, 2019, **3**, 275–290.
- 10 S. Markandeya, P. Shukla and D. Mohan, *Res. J. Environ. Toxicol.*, 2017, **11**, 72–89.
- 11 S. H. Alwan, H. A. H. Alshamsi and L. S. Jasim, *J. Mol. Struct.*, 2018, **1161**, 356–365.
- 12 F. Motahari, M. R. Mozdianfard and M. Salavati-Niasari, *Process Saf. Environ. Prot.*, 2015, **93**, 282–292.
- 13 W. Xiao, Z. N. Garba, S. Sun, I. Lawan, L. Wang, M. Lin and Z. Yuan, *J. Cleaner Prod.*, 2020, **253**, 119989.
- 14 A. Zahir, Z. Aslam, U. Aslam, A. Abdullah, R. Ali and M. M. Bello, *Chem. Biochem. Eng. Q.*, 2020, **34**, 93–104.
- 15 J. Wu, J. Yang, G. Huang, C. Xu and B. Lin, *J. Cleaner Prod.*, 2020, **251**, 119717.
- 16 G. Crini and E. Lichtfouse, *Environ. Chem. Lett.*, 2019, **17**, 145–155.
- 17 J. A. Garrido-Cardenas, B. Esteban-García, A. Agüera, J. A. Sánchez-Pérez and F. Manzano-Agugliaro, *Int. J. Environ. Res. Public Health*, 2020, **17**, 170.
- 18 T. B. T. Dao, T. T. L. Ha, T. Do Nguyen, H. N. Le, C. N. Ha-Thuc, T. M. L. Nguyen, P. Perre and D. M. Nguyen, *Chemosphere*, 2021, **280**, 130802.
- 19 A. Boughelout, N. Zebbar, R. Macaluso, Z. Zohour, A. Bensouilah, A. Zaffora, M. S. Aida, M. Kechouane and M. Trari, *Optik*, 2018, **174**, 77–85.
- 20 D. Mitoraj, U. Lamdad, W. Kangwansupamonkon, M. Pacia, W. Macyk, N. Wetchakun and R. Beranek, *J. Photochem. Photobiol., A*, 2018, **366**, 103–110.
- 21 B. O. Orimolade, A. O. Idris, U. Feleni and B. Mamba, *Environ. Pollut.*, 2021, **289**, 117891.
- 22 A. Boughelout, R. Macaluso, M. Kechouane and M. Trari, *React. Kinet., Mech. Catal.*, 2020, **129**, 1115–1130.
- 23 V. Alman, K. Singh, T. Bhat, A. Sheikh and S. Gokhale, *Appl. Phys. A: Mater. Sci. Process.*, 2020, **126**, 1–9.
- 24 P. Fernandez-Ibanez, S. McMichael, A. Rioja Cabanillas, S. Alkharabsheh, A. Tolosana Moranchel and J. A. Byrne, *Curr. Opin. Chem. Eng.*, 2021, **34**, 100725.
- 25 A. A. Al-Gheethi, Q. M. Azhar, P. Senthil Kumar, A. A. Yusuf, A. K. Al-Buriah, R. M. S. Radin Mohamed and M. M. Al-shaibani, *Chemosphere*, 2022, **287**, 132080.
- 26 A. K. Al-Buriah, A. A. Al-Gheethi, P. Senthil Kumar, R. M. S. Radin Mohamed, H. Yusof, A. F. Alsharif and N. A. Khalifa, *Chemosphere*, 2022, **287**, 132162.
- 27 X. Chen, Z. Xue, Y. Yao, W. Wang, F. Zhu and C. Hong, *Int. J. Photoenergy*, 2012, **2012**, 1–5.
- 28 S. Merouani, O. Hamdaoui, F. Saoudi, M. Chiha and C. Pétrier, *J. Hazard. Mater.*, 2010, **175**, 593–599.
- 29 M. Tuzen, A. Sari and T. A. Saleh, *J. Environ. Manage.*, 2018, **206**, 170–177.
- 30 O. Üner, Ü. Geçgel, H. Kolancilar and Y. Bayrak, *Chem. Eng. Commun.*, 2017, **204**, 772–783.
- 31 S. Singh, A. Kumar and H. Gupta, *Appl. Water Sci.*, 2020, **10**, 1–8.
- 32 E. Birtalan, B. Rudat, D. K. Kölmel, D. Fritz, S. B. L. Vollrath, U. Schepers and S. Bräse, *Biopolymers*, 2011, **96**, 694–701.
- 33 K. A. Adegoke, O. R. Adegoke, A. O. Araoye, J. Ogunmodede, O. S. Agboola and O. S. Bello, *Bioresour. Technol. Rep.*, 2022, 101082.
- 34 S. Sharma, A. L. I. Imran and others, *J. Toxicol. Environ. Health Sci.*, 2011, **3**, 286–297.
- 35 M. R. R. Kooh, L. B. L. Lim, L. H. Lim and M. K. Dahri, *Environ. Monit. Assess.*, 2016, **188**, 1–15.
- 36 K. Kannan and T. Venugopal, *Enviro Geo Chemica Acta*, 2014, **1**, 140–146.
- 37 O. Hamdaoui, *Desalination*, 2011, **271**, 279–286.
- 38 X. Gao, Y. Zhang, Y. Dai and F. Fu, *J. Solid State Chem.*, 2016, **239**, 265–273.
- 39 I. S. Yahia, Y. S. Rammah and K. F. Khaled, *J. Mater. Environ. Sci.*, 2013, **4**, 442–447.
- 40 W.-H. Su, S. A. Fennimore and D. C. Slaughter, *2020 ASABE Annual International Virtual Meeting, July 13–15, 2020*, American Society of Agricultural and Biological Engineers, St. Joseph, MI, 2020, pp. 1–10.
- 41 X. Wang, Y. Guo, Z. Jia, H. Ma, C. Liu, Z. Liu, Q. Shi, B. Ren, L. Li, X. Zhang and Y. Hu, *Desalination*, 2021, **516**, 115220.
- 42 P. Gharbani and A. Mehrizad, *Carbohydr. Polym.*, 2022, **277**, 118860.
- 43 S. Harish, P. Bharathi, P. Prasad, R. Ramesh, S. Ponnusamy, M. Shimomura, J. Archana and M. Navaneethan, *RSC Adv.*, 2021, **11**, 19283–19293.
- 44 T. T. Truong, T. T. Pham, T. T. T. Truong and T. D. Pham, *Environ. Sci. Pollut. Res.*, 2022, **29**, 22576–22588.
- 45 L. T. T. Nguyen, D. V. N. Vo, L. T. H. Nguyen, A. T. T. Duong, H. Q. Nguyen, N. M. Chu, D. T. C. Nguyen and T. Van Tran, *Environ. Technol. Innovation*, 2022, **25**, 102130.
- 46 S. Balasurya, M. K. Okla, A. Mohebalain, A. A. AL-ghamdi, M. A. Abdel-Maksoud, B. Almunqedhi, H. AbdElgawad, A. M. Thomas, L. L. Raju and S. S. Khan, *J. Environ. Manage.*, 2022, **308**, 114614.
- 47 M. A. Hamza, S. A. Abd El-Rahman and Z. M. Abou-Gamra, *Opt. Mater.*, 2022, **124**, 111987.
- 48 H. Ashiq, N. Nadeem, A. Mansha, J. Iqbal, M. Yaseen, M. Zahid and I. Shahid, *J. Phys. Chem. Solids*, 2022, **161**, 110437.
- 49 J. A. Khan, M. Sayed, S. Khan, N. S. Shah, D. D. Dionysiou and G. Boczkaj, *Contam. Emerg. Concern Water Wastewater Adv. Treat. Process.*, 2019, pp. 299–365.
- 50 N. Welter, J. Leichtweis, S. Silvestri, P. I. Z. Sánchez, A. C. C. Mejia and E. Carissimi, *J. Alloys Compd.*, 2022, **901**, 163758.
- 51 H. Xu, H. Guo, C. Chai, N. Li, X. Lin and W. Xu, *Chemosphere*, 2022, **286**, 131936.
- 52 Y. Cui, Z. Zhou, Y. Gao, L. Lei, J. Cao, R. Wu, L. Liang and Z. Huang, *J. Cleaner Prod.*, 2021, **289**, 125807.
- 53 W. H. Brattain and C. G. B. Garrett, *Bell Syst. Tech. J.*, 1955, **34**, 129–176.



- 54 A. Fujishima and K. Honda, *Nature*, 1972, **238**, 37–38.
- 55 S. Garcia-Segura and E. Brillas, *J. Photochem. Photobiol. C*, 2017, **31**, 1–35.
- 56 M. G. Peleyeju and O. A. Arotiba, *Environ. Sci.: Water Res. Technol.*, 2018, **4**, 1389–1411.
- 57 R. Dagherir, P. Drogui and D. Robert, *J. Photochem. Photobiol. A*, 2012, **238**, 41–52.
- 58 I. Sirés and E. Brillas, *Environ. Int.*, 2012, **40**, 212–229.
- 59 A. P. P. da Rosa, R. P. Cavalcante, T. F. da Silva, F. Gozzi, C. Byrne, E. McGlynn, G. A. Casagrande, S. C. de Oliveira and A. M. Junior, *J. Nanosci. Nanotechnol.*, 2019, **20**, 1177–1188.
- 60 M. A. Desai, V. Sharma, M. Prasad, S. Jadkar, G. D. Saratale and S. D. Sartale, *Int. J. Hydrogen Energy*, 2020, **45**, 5783–5792.
- 61 S. Palmas, L. Mais, M. Mascia and A. Vacca, *Curr. Opin. Electrochem.*, 2021, **28**, 100699.
- 62 O. M. Ama and O. A. Arotiba, *J. Electroanal. Chem.*, 2017, **803**, 157–164.
- 63 G. Roselló-Márquez, R. M. Fernández-Domene and J. García-Antón, *J. Electroanal. Chem.*, 2021, **894**, 115366.
- 64 S. Wu and Y. H. Hu, *Chem. Eng. J.*, 2021, **409**, 127739.
- 65 M. Jia, Z. Yang, H. Xu, P. Song, W. Xiong, J. Cao, Y. Zhang, Y. Xiang, J. Hu, C. Zhou, Y. Yang and W. Wang, *Chem. Eng. J.*, 2020, **388**, 124388.
- 66 T. F. da Silva, R. P. Cavalcante, D. R. V. Guelfi, S. C. de Oliveira, G. A. Casagrande, A. R. L. Caires, F. F. de Oliveira, J. R. Gubiani, J. C. Cardoso and A. Machulek, *J. Environ. Chem. Eng.*, 2022, **10**, 107212.
- 67 S. R. Kim, I. Ali and J. O. Kim, *Appl. Surf. Sci.*, 2019, **477**, 71–78.
- 68 R. Li, X. Zhao, X. Chen, T. Jiang, D. Y. C. Leung, D. Pan, G. Li and W. Wang, *Appl. Surf. Sci.*, 2018, **467–468**, 658–665.
- 69 B. O. Orimolade and O. A. Arotiba, *J. Electroanal. Chem.*, 2020, **878**, 114724.
- 70 E. H. Umukoro, M. G. Peleyeju, J. C. Ngila and O. A. Arotiba, *Chem. Eng. J.*, 2017, **317**, 290–301.
- 71 E. H. Umukoro, N. Kumar, J. C. Ngila and O. A. Arotiba, *J. Electroanal. Chem.*, 2018, **827**, 193–203.
- 72 S. Sun, W. Wang and L. Zhang, *J. Phys. Chem. C*, 2012, **116**, 19413–19418.
- 73 D. Cao, Y. Wang, M. Qiao and X. Zhao, *J. Catal.*, 2018, **360**, 240–249.
- 74 Q. Ma, H. Wang, H. Zhang, X. Cheng, M. Xie and Q. Cheng, *Sep. Purif. Technol.*, 2017, **189**, 193–203.
- 75 B. A. Koiki, B. O. Orimolade, B. N. Zwane, D. Nkosi, N. Mabuba and O. A. Arotiba, *Electrochim. Acta*, 2020, **340**, 135944.
- 76 B. O. Orimolade, B. A. Koiki, B. N. Zwane, G. M. Peleyeju, N. Mabuba and O. A. Arotiba, *RSC Adv.*, 2019, **9**, 16586–16595.
- 77 A. Bacha, I. Nabi, H. Cheng, K. Li, S. Ajmal and T. Wang, *Chem. Eng. J.*, 2020, **389**, 124482.
- 78 Y. Liu, Y. Li, W. Li, S. Han and C. Liu, *Appl. Surf. Sci.*, 2012, **258**, 5038–5045.
- 79 L. Zhang and M. Jaroniec, *Appl. Surf. Sci.*, 2018, **430**, 2–17.
- 80 H. Du, W. Pu, Y. Wang, K. Yan, J. Feng, J. Zhang, C. Yang and J. Gong, *J. Alloys Compd.*, 2019, **787**, 284–294.
- 81 S. Adhikari, S. Selvaraj and D. H. Kim, *Appl. Catal., B*, 2019, **244**, 11–24.
- 82 L. Cheng, Y. Tian and J. Zhang, *J. Colloid Interface Sci.*, 2018, **526**, 470–479.
- 83 B. O. Orimolade and O. A. Arotiba, *Sci. Rep.*, 2020, **10**, 1–13.
- 84 R. S. Pedaneekar, S. B. Madake, N. A. Narewadikar, S. V. Mohite, A. R. Patil, S. M. Kumbhar and K. Y. Rajpure, *Mater. Res. Bull.*, 2022, **147**, 111639.
- 85 E. Amaterz, A. Bouddouch, A. Tara, A. Taoufyq, Z. Anfar, B. Bakiz, L. Bazzi, A. Benlhachemi and O. Jbara, *Electrocatalysis*, 2020, **11**, 642–654.
- 86 Y. Zhou, X. Fan, G. Zhang and W. Dong, *Chem. Eng. J.*, 2019, **356**, 1003–1013.
- 87 Y. Zhou, G. Zhang and J. Zou, *Water Reuse*, 2021, **11**, 531–541.
- 88 Y. Shao, K. Feng, J. Guo, R. Zhang, S. He, X. Wei, Y. Lin, Z. Ye and K. Chen, *J. Adv. Ceram.*, 2021, **10**, 1025–1041.
- 89 Y. Wang, M. Zu, X. Zhou, H. Lin, F. Peng and S. Zhang, *Chem. Eng. J.*, 2020, **381**, 122605.
- 90 R. Y. N. Reis, A. E. B. Lima, M. J. S. Costa, J. F. Cruz-Filho, J. P. C. Moura, R. S. Santos and G. E. Luz, *Surf. Interfaces*, 2020, **21**, 100675.
- 91 H. Kiziltas, *Opt. Mater.*, 2022, **123**, 111926.
- 92 M. Z. Muzakkar, A. A. Umar, I. Ilham, Z. Saputra, L. Zulfikar, M. Maulidiyah, D. Wibowo, R. Ruslan and M. Nurdin, *J. Phys.: Conf. Ser.*, 2019, **1242**, 012016.
- 93 C. Wu, Z. Gao, S. Gao, Q. Wang, H. Xu, Z. Wang, B. Huang and Y. Dai, *J. Energy Chem.*, 2016, **25**, 726–733.
- 94 M. Nurdin, D. Wibowo, T. Azis, R. A. Safitri, M. Maulidiyah, A. Mahmud, F. Mustapa, R. Ruslan, L. O. Agus Salim, Z. Arham and A. A. Umar, *Surf. Eng. Appl. Electrochem.*, 2022, **58**, 125–134.
- 95 V. P. Kothavale, T. S. Patil, P. B. Patil and C. H. Bhosale, *Mater. Today: Proc.*, 2020, **23**, 382–388.
- 96 T. Jiang, L. Cheng, Y. Han, J. Feng and J. Zhang, *Sep. Purif. Technol.*, 2019, **238**, 116428.
- 97 M. Ma, E. Lei, D. Zhao, Y. Xin, X. Wu, Y. Meng and Z. Liu, *Colloids Surf., A*, 2022, **633**, 127834.
- 98 İ. Ç. Davaslıoğlu, K. Volkan Özdokur, S. Koçak, Ç. Çırak, B. Çağlar, B. B. Çırak and F. Nil Ertaş, *J. Mol. Struct.*, 2021, **1241**, 130673.
- 99 B. O. Orimolade, B. A. Koiki, B. N. Zwane, G. M. Peleyeju, N. Mabuba and O. A. Arotiba, *RSC Adv.*, 2019, **9**, 16586–16595.
- 100 H. Wang, Y. Liang, L. Liu, J. Hu and W. Cui, *Appl. Surf. Sci.*, 2017, **392**, 51–60.
- 101 Z. Liu, Q. Wang, W. Rong, R. Jin, Y. Cui and S. Gao, *Sep. Purif. Technol.*, 2018, **200**, 191–197.
- 102 Y.-C. Liang and T.-H. Li, *Nanotechnol. Rev.*, 2021, **11**, 284–297.
- 103 E. Amaterz, A. Tara, A. Bouddouch, A. Taoufyq, B. Bakiz, F. Lazar, M. Gilliot, A. Benlhachemi, L. Bazzi and O. Jbara, *J. Appl. Electrochem.*, 2020, **50**, 569–581.



## Review

- 104 A. Ait hssi, E. Amaterz, N. Labchir, L. Atourki, I. Y. Bouderbala, A. Elfanaoui, A. Benlhachemi, A. Ihlal and K. Bouabid, *Phys. Status Solidi*, 2020, **217**, 2000349.
- 105 A. Chennah, E. Amaterz, A. Taoufyq, B. Bakiz, Y. Kadmi, L. Bazzi, F. Guinneton, J.-R. Gavarrri and A. Benlhachemi, *Process Saf. Environ. Prot.*, 2021, **148**, 200–209.
- 106 X. Hou, X. Liu, J. Han, H. Liu, J. Yao, D. Li, L. Wang, B. Liao, J. Li and R. Zhang, *J. Mater. Sci.*, 2020, **55**, 5843–5860.
- 107 H.-J. Chen, Y.-L. Yang, M. Hong, J.-G. Chen, G.-Q. Suo, X.-J. Hou, L. Feng and Z.-G. Chen, *Sustainable Mater. Technol.*, 2019, **21**, e00105.
- 108 S. Han, W. i Qu, J. Xu, D. Wu, Z. Shi, Z. Wen and Y. Tian, *Phys. Status Solidi*, 2017, **214**, 1700059.
- 109 D. Jia, J. Yu, S. M. Long and H. L. Tang, *Water Sci. Technol.*, 2018, **2017**, 752–761.
- 110 D. Zhao, A. Li, M. Wu and M. Du, *React. Kinet., Mech. Catal.*, 2018, **124**, 347–362.
- 111 Y. M. Hunge, A. A. Yadav, M. A. Mahadik, R. N. Bulakhe, J. J. Shim, V. L. Mathe and C. H. Bhosale, *Opt. Mater.*, 2018, **76**, 260–270.
- 112 Q. Wang, C. Sun, Z. Liu, X. Tan, S. Zheng, H. Zhang, Y. Wang and S. Gao, *Mater. Res. Bull.*, 2019, **111**, 277–283.
- 113 Y. Wang, N. Lu, M. Luo, L. Fan, K. Zhao, J. Qu, J. Guan and X. Yuan, *Appl. Surf. Sci.*, 2019, **463**, 234–243.
- 114 Z. Liu, Y. Song, Q. Wang, Y. Jia, X. Tan, X. Du and S. Gao, *J. Colloid Interface Sci.*, 2019, **556**, 92–101.
- 115 T. Jiang, L. Cheng, Y. Han, J. Feng and J. Zhang, *Sep. Purif. Technol.*, 2020, **238**, 116428.
- 116 D. Zhao, F. C. Dai, A. C. Li, Y. Chen, G. H. Li, Q. Wang, W. S. Hou and H. Z. Zhou, *New J. Chem.*, 2020, **44**, 9502–9508.
- 117 W. Chen, J. Huang, X. Yu, X. Fu, Y. Zhu and Y. Zhang, *J. Solid State Chem.*, 2020, **289**, 121480.
- 118 W. Nareejun and C. Ponchio, *Sol. Energy Mater. Sol. Cells*, 2020, **212**, 110556.
- 119 J. P. C. Moura, R. Y. N. Reis, A. E. B. Lima, R. S. Santos and G. E. Luz, *J. Photochem. Photobiol., A*, 2020, **401**, 112778.
- 120 Z. Zhang, C. Zhao, S. Lin, H. Li, Y. Feng and X. Gao, *Fuel*, 2021, **285**, 119171.
- 121 Y.-C. Liang and C.-H. Huang, *Nanotechnol. Rev.*, 2022, **11**, 1248–1262.

